Delayed feedback control of forced self-sustained oscillations

T. Pyragienė and K. Pyragas*
Semiconductor Physics Institute, LT-011088 Vilnius, Lithuania
(Received 4 March 2005; published 3 August 2005)

We consider a weakly nonlinear van der Pol oscillator subjected to a periodic force and delayed feedback control. Without control, the oscillator can be synchronized by the periodic force only in a certain domain of parameters. However, outside of this domain the system possesses unstable periodic orbits that can be stabilized by delayed feedback perturbation. The feedback perturbation vanishes if the stabilization is successful and thus the domain of synchronization can be extended with only small control force. We take advantage of the fact that the system is close to a Hopf bifurcation and derive a simplified averaged equation which we are able to treat analytically even in the presence of the delayed feedback. As a result we obtain simple analytical expressions defining the domain of synchronization of the controlled system as well as an optimal value of the control gain. The analytical theory is supported by numerical simulations of the original delay-differential equations.

DOI: 10.1103/PhysRevE.72.026203 PACS number(s): 05.45.Gg, 02.30.Yy, 02.30.Ks

I. INTRODUCTION

Although the delayed feedback control (DFC) method has been introduced more than one decade ago [1] it is still one of the most active fields in applied nonlinear science [2,3]. The method allows a noninvasive stabilization of unstable periodic orbits (UPO's) of dynamical systems in the sense that the control force vanishes when the target state is reached. The DFC is reference-free; it makes use of a control signal obtained from the difference between the current state of the system and the state of the system delayed by one period of the unstable orbit. Such a scheme is especially superior for fast dynamical systems, since it does not require any real-time computer processing. Successful implementation of this algorithm has been attained in diverse experimental systems, including electronic chaotic oscillators [4], mechanical pendulums [5], lasers [6], gas discharge systems [7], a current-driven ion acoustic instability [8], a chaotic Taylor-Couette flow [9], chemical systems [10], high-power ferromagnetic resonance [11], helicopter rotor blades [12], and a cardiac system [13].

Several variants of the original delayed feedback scheme have been proposed to improve the control performance. Among those are extended DFC (EDFC) schemes employing multiple delays to stabilize strongly unstable orbits [14,15] or unstable DFC (UDFC) schemes using an unstable degree of freedom in a feedback loop [16,17] to overcome the so-called odd number limitation from which usual delayed feedback control suffers [18].

Most investigations in the theory of delayed feedback control are devoted to the stabilization of unstable periodic orbits embedded in chaotic attractors of low-dimensional (usually three-dimensional) systems. The leading Floquet multipliers of such orbits are real-valued and lay outside the unit circle in the complex plane [Figs. 1(a) and 1(b)]. The orbits with the negative real multiplier arise from a period-doubling bifurcation and are typical, for example, for the Rössler system or periodically driven Duffing oscillator. The mechanism of stabilization of such orbits by delayed feedback is well understood [19,20]. The orbits with the positive real multiplier come from a tangent bifurcation and are typical, for example, for the Lorenz system. They satisfy the odd number limitation and cannot be stabilized by the usual delayed feedback method. The mechanism of stabilization of such orbits by the UDFC is described in Ref. [16]. Recently we have developed an analytical approach for the UDFC method when the system is close to a subcritical Hopf bifurcation [17].

In addition to the above mentioned orbits there exists a large class of unstable periodic orbits with the complex conjugate pair of leading Floquet multipliers [Fig. 1(c)]. Such orbits arise from a Nejmark-Sacker (discrete Hopf) bifurcation and cannot appear in low-dimensional chaotic attractors. Presumably for this reason they have not been considered in delayed feedback control theory so far. However, such orbits may appear in low-dimensional nonchaotic systems. The intent of this paper is to consider the control of such orbits. Note that all three types of orbits have different topological properties. The orbits with the negative real multiplier flip their neighborhood during one turn. The orbits with the positive real multiplier have no torsion, and finally the orbits with the complex conjugate pair of the multipliers have a finite torsion.

In this paper, we consider the problem of controlling synchronization in a forced self-sustained oscillator. Very often

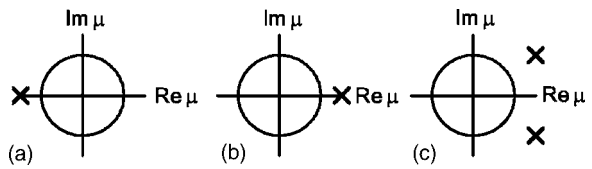

FIG. 1. Leading Floquet multipliers of unstable periodic orbits arising from different bifurcations: (a) period doubling, (b) tangent, and (c) Nejmark-Sacker (discrete Hopf) bifurcations. The unit circle defines the region of stability.

*Electronic address: pyragas@pfi.lt; http://pyragas.pfi.lt

in practical application the need arises to control the properties of oscillations. Usually control assumes an enhancement in regularity of motion. Suppose that our aim is to maintain the synchronous regime of a periodically driven self-sustained oscillator. Due to drift of parameters the desired synchronization may be lost and a kind of beat phenomenon may occur. We imagine that the external force driving the oscillator is inaccessible in experiment, but we can measure an output of the oscillator and can control its state through some accessible input. Then applying the delayed feedback control we can return the system to the synchronized state. In this paper, we demonstrate these ideas for the van der Pol oscillator.

The rest of the paper is organized as follows. In Sec. II, we derive averaged equations for the controlled van der Pol oscillator and analyze unstable periodic orbits of the uncontrolled system. In Sec. III, we investigate a linear stability of the unstable periodic orbits controlled by delayed feedback. Section IV is devoted to the extended delayed feedback controller. In Sec. V, we demonstrate the results of numerical simulations of the original delay-differential equations. The paper is finished with conclusions presented in Sec. VI.

II. AVERAGED EQUATION AND UNSTABLE ORBITS OF UNCONTROLLED SYSTEM

A. Problem formulation and averaged equation

Consider a weakly nonlinear van der Pol oscillator under action of external periodic force and delayed feedback perturbation

$$\ddot{x} + \omega_0^2 x + \varepsilon(x^2 - 1)\dot{x} = a\sin(\omega t) + k(x - x_T). \tag{1}$$

The left-hand side represents the standard van der Pol equation. The parameter ω_0 is the characteristic frequency of self-sustained oscillations, and ε is responsible for the strength of nonlinearity of the oscillator. The first term in the right-hand side is an external periodic force (a is the amplitude and ω is the frequency) and the second term describes the delayed coupling due to control. The parameter k is the feedback gain, $x_T \equiv x(t-T)$, and $T=2\pi/\omega$ is the period of the external force. In the following we consider Eq. (1) as a weakly nonlinear system. Specifically, we suppose that ε is a small parameter, $\varepsilon \ll \omega_0$. Moreover we assume that the amplitude a, the frequency detuning $\omega-\omega_0$ as well as the control perturbation $k(x-x_T)$ are proportional to the small parameter ε.

For weakly nonlinear systems, there are many mathematically rigorous ways (e.g., method of averaging, multiscale expansion, and other asymptotic methods) to obtain approximate solutions. We will apply the method of averaging. First we rewrite Eq. (1) as a system

$$\dot{x} = y, \tag{2a}$$

$$\dot{y} = -\omega_0^2 x - \varepsilon(x^2 - 1)y + a\sin(\omega t) + k(x - x_T). \tag{2b}$$

As Eq. (1) or system (2) is close to that of linear oscillator, we can expect that the solution has a nearly harmonic form. Since there is a forced system we look for a solution with the characteristic frequency ω

$$x = (A(t)e^{i\omega t} + A^*(t)e^{-i\omega t})/2. \tag{3}$$

Here $A(t)$ is a new variable, a slowly varying complex amplitude. Since it is complex, we need two relations to have one-to-one correspondence between (x,y) and A. It is convenient to introduce the following relation between y and A:

$$y = i\omega(A(t)e^{i\omega t} - A^*(t)e^{-i\omega t})/2. \tag{4}$$

Substituting Eqs. (3) and (4) in system (2) we obtain the equation for the complex amplitude, which after averaging over the period T of fast oscillations takes the form

$$\dot{A} = \frac{\omega^2 - \omega_0^2}{2i\omega}A - \frac{\varepsilon}{2}A\left(\frac{|A|^2}{4} - 1\right) - \frac{a}{2\omega} + \frac{k}{2i\omega}(A - A_T). \tag{5}$$

By choosing an appropriate scale for the amplitude

$$A = 2z \tag{6}$$

and introducing new parameters

$$\alpha = \frac{a}{2\varepsilon\omega}, \quad \nu = \frac{\omega^2 - \omega_0^2}{\varepsilon\omega} \approx 2\frac{\omega - \omega_0}{\varepsilon}, \quad \kappa = \frac{k}{\varepsilon\omega} \tag{7}$$

Eq. (5) can be simplified to

$$(2/\varepsilon)\dot{z} = -i\nu z - z(|z|^2 - 1) - \alpha - i\kappa(z - z_T). \tag{8}$$

The parameters α, ν, and κ are proportional respectively to the amplitude of external force, the frequency detuning, and the delayed feedback gain.

B. Periodic orbits of the system

We now determine the steady state solutions of the uncontrolled system ($\kappa=0$) and analyze their stability. A similar analysis is presented in many textbooks, however most attention is usually concentrated on the stable solutions describing the synchronized states. In our consideration we focus on unstable periodic orbits. In the following sections they will be the subject of the delayed feedback control.

The (approximate) bifurcation diagram of Eq. (8) for $\kappa=0$ is shown in Fig. 2. Since it is symmetrical with respect to the ν and α axis, only the part $\nu \geqslant 0$, $\alpha \geqslant 0$ is presented. We start the analysis with finding the stationary solutions. Setting $\dot{z}=0$ and $z=z_0$, we obtain

$$-i\nu z_0 - z_0(|z_0|^2 - 1) - \alpha = 0. \tag{9}$$

We introduce the notations

$$s = |z_0|^2, \quad f_\nu(s) = s[(s-1)^2 + \nu^2]. \tag{10}$$

Then the values of s can be found by solving the cubic equation

$$f_\nu(s) = \alpha^2 \tag{11}$$

with respect to s. Knowing s, from Eq. (9) one can determine the steady state value of z,

$$z_0 = -\alpha/(s - 1 + i\nu). \tag{12}$$

Solutions of the cubic Eq. (11) define stationary periodic orbits of the forced system. The period of these orbits coin-

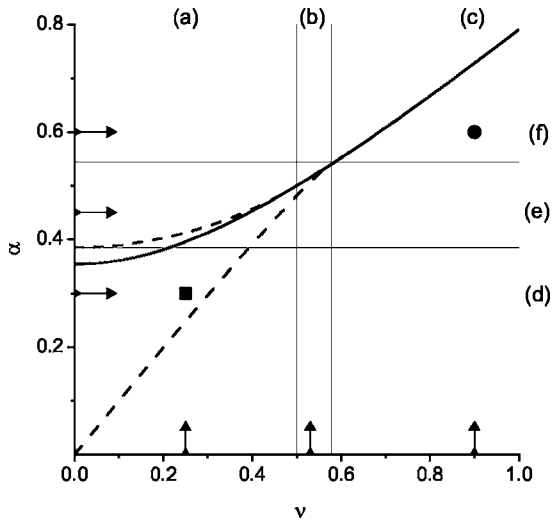

FIG. 2. The bifurcation diagram for the uncontrolled van der Pol oscillator. The broken lines are defined by Eq. (14b). The region between these lines correspondsto three periodic orbits. Outside this region there is only one periodic orbit. The thick solid line is the hyperbola (17) defining the Hopf bifurcation. The vertical lines divide the diagram into three regions: (a) $\nu^2<1/4$, (b) $1/4<\nu^2<1/3$, and (c) $1/3<\nu^2$. By horizontal lines the diagram is divided into regions (d) $\alpha^2<4/27$, (e) $4/27<\alpha^2<8/27$, and (f) $8/27<\alpha^2$. The vertical [horizontal] arrows show the fixed values of the parameter ν [α] taken from regions (a), (b), and (c) [(d), (e), and (f)] for which the $|A_0|$ vs α [$|A_0|$ vs ν] characteristics are presented in Figs. 3(a)–3(c) and [Figs. 3(d)–3(f)], respectively. The solid dot $(\nu,\alpha)=(0.9,0.6)$ and square $(\nu,\alpha)=(0.25,0.3)$ show the sets of parameters which will be used in the following analysis to demonstrate the delayed feedback control performance.

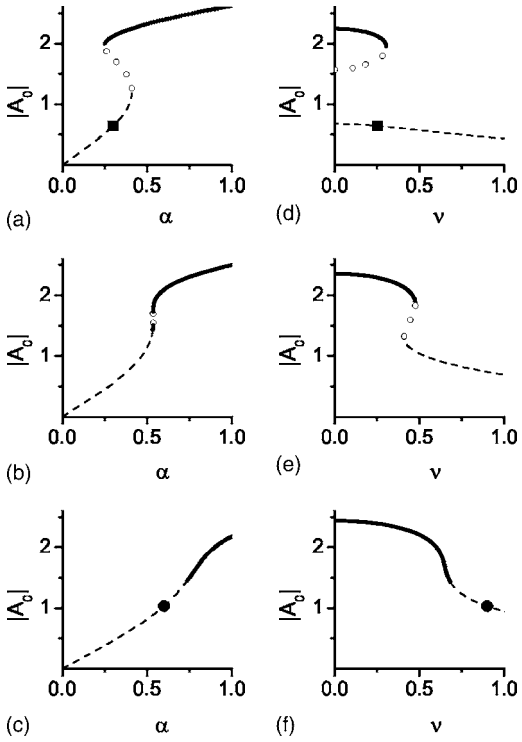

FIG. 3. The amplitude $|A_0|$ of the periodic orbit as function of the amplitude α of the external force for the fixed value of the detuning (a) $\nu=0.25$, (b) $\nu=0.53$, (c) $\nu=0.9$, and as function of the detuning ν for the fixed value of the amplitude of the external force (d) $\alpha=0.3$, (e) $\alpha=0.46$, (f) $\alpha=0.6$. Solid lines denote the stable orbits, open circles represent the saddle orbits, and dashed lines show unstable periodic orbits with a pair of complex conjugate Floquet exponents. Solid dots and squares mark the same set of the parameters (ν,α) as in Fig. 2.

cides with the period T of the external force, and the amplitude [the radius in the (x,y) plane] is

$$|A_0| = 2|z_0| = 2\sqrt{s}. \tag{13}$$

Equation (11) has three real roots provided

$$\alpha_1^2(\nu) < \alpha^2 < \alpha_2^2(\nu), \tag{14a}$$

$$\alpha_{1,2}^2(\nu) = \frac{2}{27}[9\nu^2 + 1 \mp (1-3\nu^2)^{3/2}] \tag{14b}$$

or one real root otherwise. Thus the forced van der Pol oscillator has either three or one periodic orbit(s). The region with three orbits is between broken lines in Fig. 2. Outside this region there is only one periodic orbit.

From a physical point of view it is interesting to investigate the bifurcations for two different cases, namely (i) for a fixed detuning ν and variable amplitude of external force α, or (ii) for a fixed α and variable ν. For the first case, the thin vertical lines divide the bifurcation diagram into three regions [(a), (b), and (c)] with different behavior. The $|A_0|$ vs α characteristics in these three regions are, respectively, shown in Figs. 3(a)–3(c). Similarly, for the second case the bifurcation diagram is divided into three regions [(e), (f), and (g)] by horizontal lines for which the $|A_0|$ vs ν characteristics are respectively presented in Figs. 3(e)–3(g). Typical evolution of the periodic orbits in the (x,y) plane is shown in Fig. 4.

To determine the stability of periodic orbits, we have to linearize Eq. (8), which leads to the characteristic equation

$$\left(\frac{2\lambda}{\varepsilon}\right)^2 - 2(1-2s)\frac{2\lambda}{\varepsilon} + f_\nu'(s) = 0. \tag{15}$$

Here λ is the Floquet exponent (FE) of the periodic orbit, s is the solution of the cubic equation (11), and

$$f_\nu'(s) = (3s-1)(s-1) + \nu^2 \tag{16}$$

is the derivative of the function $f_\nu(s)$ defined in Eq. (10). The stability of a periodic orbit depends on the value of s or, due to the relation (13) $|A_0|=2\sqrt{s}$, on the amplitude of the orbit.

Two different types of bifurcations may occur in the system. For $f_\nu'(s)=0$ we have a tangent (saddle-node) bifurcation, and for $s=1/2$ a Hopf bifurcation arises. The condition $f_\nu'(s)=0$ defines the boundaries $\alpha^2=\alpha_{1,2}^2(\nu)$ of the region with three periodic orbits in the (ν,α) plane (broken lines in Fig. 2). When crossing into this region two additional orbits of saddle and node types occur. The saddle orbit has two real FE's of different signs. The positive exponent $\lambda>0$ corresponds to the real positive Floquet multiplier $\mu=e^{\lambda T}>1$ and thus this orbit satisfies the odd number property. Such an

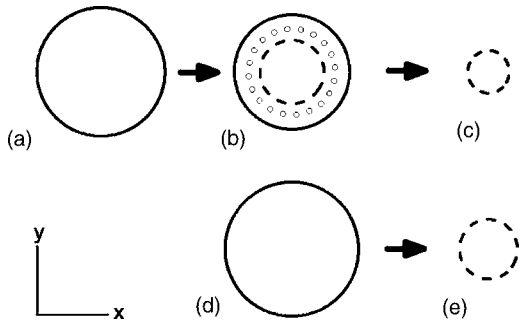

FIG. 4. Typical evolution of periodic orbits in the (x,y) plane. As well as in Fig. 3 solid lines, open circles, and dashed lines show, respectively, stable, saddle-type, and unstable (with a pair of complex conjugate FE's) orbits. The scenario (a)$\rightarrow$(b)$\rightarrow$(c) is typical when passing the region with three solutions [see Figs. 3(a) and 3(e)]. After two saddle-node bifurcations the stable orbit is replaced by an unstable one. The scenario (d)$\rightarrow$(e) represents the Hopf bifurcation [see Figs. 3(c) and 3(f)].

orbit cannot be stabilized by the usual delayed feedback method and we do not consider its control in this paper. The saddle orbits are marked by open circles in Figs. 3 and 4.

The condition of the Hopf bifurcation $s=1/2$ defines the minimal amplitude of the stable orbit $A_{\min}=\sqrt{2}$. The orbits with amplitude $|A_0|<A_{\min}$ are unstable. In the (ν,α) plane, this condition defines the hyperbola

$$\alpha^2 = f_\nu(1/2) = \nu^2/2 + 1/8, \tag{17}$$

which is shown by a solid line in Fig. 2. Above this line the oscillator is synchronized with the external force; the phase of the oscillator is locked by the phase of the external force and its amplitude is independent of time. Below this line, in the region of a single solution, the stability of the periodic orbit with the frequency ω is lost and we usually have a quasiperiodic behavior. The orbits losing their stability through the Hopf bifurcation [scenario (d)$\rightarrow$(e) in Fig. 4] have a pair of complex conjugate exponents with the positive real part. Similar properties have one of the orbits arising from the saddle-node bifurcation [scenario (a)$\rightarrow$(b)$\rightarrow$(c) in Fig. 4]. Unstable orbits having a pair of complex conjugate exponents with the positive real part are marked by dashed lines in Figs. 3 and 4. In the next section we analyze their stability under action of the delayed feedback control.

III. LINEAR STABILITY OF THE SYSTEM CONTROLLED BY DELAYED FEEDBACK

We now analyze Eq. (8) for $\kappa\neq 0$. The term $\kappa(z-z_T)$ does not change the steady state solutions of this equation, but can change their stability. Thus the delayed feedback can noninvasively influence the frequency entrainment condition. The characteristic equation now reads

$$\left(\frac{2\lambda}{\varepsilon}\right)^2 - 2(1-2s)\frac{2\lambda}{\varepsilon} + (3s-1)(s-1) + [\nu+\kappa(1-e^{-\lambda T})]^2 = 0. \tag{18}$$

In a general way, this is a rather complex transcendental

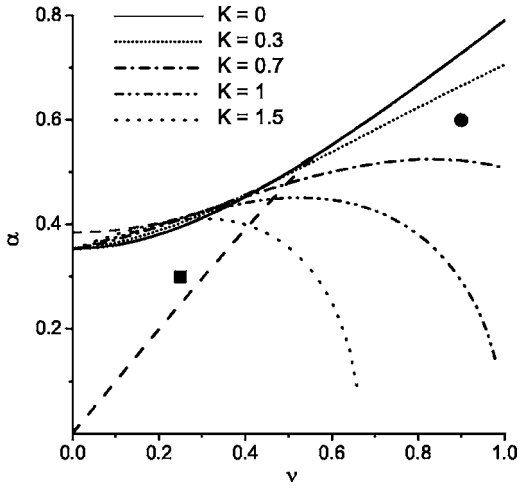

FIG. 5. The bifurcation diagram for van der Pol oscillator controlled by delayed feedback. The solid line defines the Hopf bifurcation for the uncontrolled system (the same as in Fig. 2), and broken lines are defined by Eq. (22). Above these lines the oscillator is synchronized with the external force.

equation that has an infinite number of solutions. However, we can expect that close to the Hopf bifurcation the leading Floquet exponents will be proportional to the small parameter ε. This assumption allows the approximation $e^{-\lambda T}\approx 1-\lambda T$, which simplifies Eq. (18),

$$(1+K^2)\left(\frac{2\lambda}{\varepsilon}\right)^2 - 2(1-2s-\nu K)\frac{2\lambda}{\varepsilon} + f'_\nu(s) = 0. \tag{19}$$

Here we use the notation

$$K = \kappa T\varepsilon/2 = k\pi/\omega^2. \tag{20}$$

This approximation is equivalent to that of replacing the delay term in Eq. (8) by the first derivative, $z_T=z(t-T)\approx z(t)-T\dot{z}$. Such an approximation transforms the delay-differential equation (8) to the ordinary

$$(2/\varepsilon + i\kappa T)\dot{z} = -i\nu z - z(|z|^2-1) - \alpha. \tag{21}$$

After linearization it yields Eq. (19).

From Eq. (19) we see that the delayed feedback changes the condition of the Hopf bifurcation, $1-2s-\nu K=0$, which now depends on the delayed feedback strength K. At the bifurcation point we have $s=(1-\nu K)/2$. Substituting this in Eq. (11) and using Eq. (10) we obtain the relation between K, ν, and α,

$$\alpha^2 = \tfrac{1}{8}(1-\nu K)[(1+\nu K)^2 + 4\nu^2]. \tag{22}$$

In Fig. 5, these relations are presented by curves in the (ν,α) plane for different fixed values of K. These curves define the boundaries of synchronization for the controlled oscillator. Above these curves the oscillator is synchronized with the periodic force. We see that the delayed feedback perturbation extends the phase locked domain in the Arnold tongue.

For a fixed value of the parameters (ν,α), the threshold of the feedback strength at which the Hopf bifurcation occurs is $K_0=(1-2s)/\nu$, where s satisfy the cubic equation (11). Employing Eq. (20) and relation $s=|A_0|^2/4$ the threshold can be presented in the form

$$k_0=\frac{\omega^2}{\pi}K_0=\frac{\omega^2}{\pi\nu}\left(1-\frac{|A_0|^2}{2}\right). \tag{23}$$

To demonstrate how the Floquet exponents depend on the control gain k we specify the parameters (ν,α) to be (0.9, 0.6). This set of parameters is marked by solid dots in Figs. 2, 3, and 5. We have calculated the leading Floquet exponents of the initially unstable orbit using three different methods, namely, (i) solving transcendental equation (18), (ii) using quadratic equation (19), and (iii) solving exact (nonaveraged) linearized system (2). Equation (18) has been solved by the Newton-Raphson algorithm. The third method is based on the numerical analysis of the variational equations

$$\delta\dot{x}=\delta y, \tag{24a}$$

$$\delta\dot{y}=-(\omega_0^2-2\varepsilon x_0y_0)\delta x-\varepsilon(x_0^2-1)\delta y+k(\delta x-\delta x_T). \tag{24b}$$

derived from the system (2). Here $\delta x=x-x_0(t)$, $\delta y=y-y_0(t)$ are small deviations from the unstable periodic orbit $[x_0(t),y_0(t)]=[x_0(t+T),y_0(t+T)]$ that satisfies the uncontrolled system (2). The leading Lyapunov exponents of this system have been calculated according to the algorithm described in Ref. 15. Note that the Lyapunov exponent of a periodic orbit coincides with the real part of the Floquet exponent.

The results of the above analysis for two different values of the parameter ε equal to 0.01 and 0.1 are presented in Fig. 6. The exact values of the leading FE's determined from Eq. (24) are shown by dots. There are two branches (the left-hand and the right-hand) defining the interval of stability $k_0<k<k_1$ in which the real part of the leading FE is negative. The parameters k_0 and k_1 denote the lower and upper control thresholds, respectively.

First we discuss the results for the left-hand branch. For $\varepsilon=0.01$, all three above methods give quantitatively coinciding results [Fig. 6(a)]. Thus for small ε the leading FE of the left-hand branch can be reliably obtained from the simple quadratic equation (19), which yields

$$\mathrm{Re}\,\lambda=\frac{\varepsilon}{2}\frac{1-|A_0|^2/2-\nu k\pi/\omega^2}{1+(k\pi/\omega^2)^2}, \tag{25}$$

and the threshold k_0 of the Hopf bifurcation is well described by Eq. (23). The transcendental equation (18) gives good results even for $\varepsilon=0.1$, while Eqs. (19) or (25) are less appropriate [Fig. 6(c)].

The right-hand branch of the FE defining the upper threshold k_1 cannot be quantitatively well described by Eq. (18). This is because the term $k(x-x_T)$ responsible for the control in the system (2) is not small in this case, and the averaging procedure performed with this system is not valid.

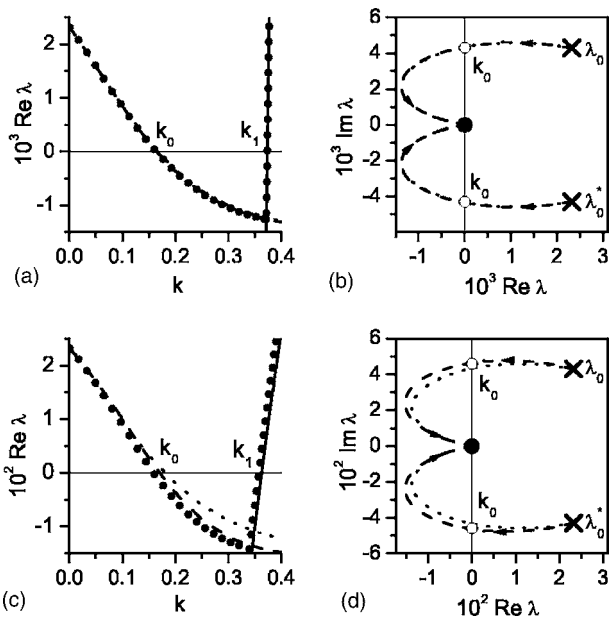

FIG. 6. Leading Floquet exponents as functions of the control gain for $(\nu,\alpha)=(0.9,0.6)$. Here and in all numerical demonstrations below we take $\omega_0=1$. By this is meant that ω, ε, and λ are measured in units of ω_0, time t is measured in units of ω_0^{-1}, and k is measured in units of ω_0^2. (a) Re λ vs k for $\varepsilon=0.01$. For the given values of parameters ν, α, and ε, we have $\omega\approx1.00451$ and $a\approx0.01205$. The amplitude of the unstable orbit is $|A_0|\approx1.034$ and its FE's for $k=0$ are $\lambda_0\approx(2.327\pm4.297i)\times10^{-3}$. Solid dots are the values of the Lyapunov exponents obtained from exact variational equations (24). The dashed and dotted lines calculated, respectively, from Eq. (18) and Eq. (19) [or Eq. (25)] approximate to the left-hand branch. The solid line calculated from Eq. (28) approximates the right-hand branch. (b) Root loci of Eq. (18) (dotted line) and Eq. (19) (dashed line) as k varies from 0 to ∞ for the same parameter value as in (a). Crosses and black dot denote the location of the roots for $k=0$ and $k=\infty$, respectively. (c) and (d) Same diagrams as in (a) and (b) but for $\varepsilon=0.1$. The parameters now are $\omega\approx1.04601$, $a\approx0.12552$, $|A_0|\approx1.034$, and $\lambda_0\approx(2.327\pm4.297i)\times10^{-2}$.

Nevertheless, we can find an approximate analytical expression for the FE using exact (nonaveraged) variational equations (24). For the right-hand branch, the nonlinear terms in Eq. (18) are small in comparison with the control term. Thus in the variational equations we can neglect the terms containing ε. Setting $\varepsilon=0$ in Eq. (24) we obtain the characteristic equation

$$\lambda^2+\omega_0^2-k(1-e^{-\lambda T})=0. \tag{26}$$

Root loci diagram of the relevant branch for this equation when varying k is shown in Fig. 7(a). The pair of complex conjugate roots intersects the imaginary axes at the points $\lambda=\pm i\pi/T=\pm i\omega/2$. This intersection appears for $k=k_1$, where

$$k_1=\frac{1}{2}\left(\omega_0^2-\frac{\omega^2}{4}\right). \tag{27}$$

defines the upper threshold of stability. For $k=k_1$, the orbit loses stability by a period doubling bifurcation since the in-

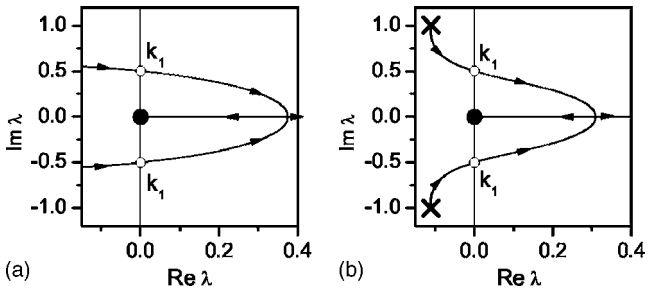

FIG. 7. Root loci of (a) Eq. (26) for $\omega=1.00451$ ($\omega_0=1$) and (b) Eq. (37) for the same ω and $R=0.5$. Crosses and black dot denote the location of the roots for $k=0$ and $k=\infty$, respectively.

tersection of the imaginary axes appears at a half frequency of the external force, $\lambda=\pm i\omega/2$. Expanding the solution of Eq. (26) in Taylor series close to the threshold $k=k_1$, we obtain an approximate analytical expression

$$\mathrm{Re}\,\lambda=\frac{4\pi k_1/\omega}{\omega^2+(2\pi k_1/\omega)^2}(k-k_1) \tag{28}$$

that describes well the $\mathrm{Re}\,\lambda$ vs k dependence for the right-hand branch [Figs. 6(a) and 6(c)].

Having analytical expressions for the left-hand [Eq. (25)] and right-hand [Eq. (28)] branches one can easily evaluate an optimal value k_{op} of the control gain that provides the minimal $\mathrm{Re}\,\lambda$ and thus the fastest convergence to the desired orbit. This value is defined by a simple intersection of these two branches and can be found from a cubic equation with respect to k, which results from equating Eqs. (25) and (28).

IV. CONTROL VIA EXTENDED DELAYED FEEDBACK

In this section, we consider a more general (extended) version of the delayed feedback control, the EDFC, that employs multiple delays [14]. An application of the EDFC to the van der Pol oscillator consists in replacing the delay term x_T in Eq. (1) or system (2) by an infinite sum over past states, namely

$$x_T \Rightarrow (1-R)\sigma_T^x, \tag{29a}$$

$$\sigma_T^x \equiv \sigma^x(t-T)=\sum_{n=1}^{\infty} R^{n-1}x(t-nT). \tag{29b}$$

The sum σ_T^x represents a geometric series with the parameter $|R|<1$ that determines the relative importance of past states. The EDFC control force $k[x-(1-R)\sigma_T^x]$ vanishes if an UPO with the period T is stabilized, as it is for the DFC. For $R=0$, we have $\sigma_T^x=x(t-T)=x_T$ and the EDFC transforms to the original DFC. The extended method is superior to the original in that it can stabilize strongly unstable orbits. In experiment, the infinite sum in Eq. (29) can be generated by a Fabry-Perot interferometer using only single time-delay element in the feedback loop [14]. When performing numerical simulations with the EDFC it is convenient to present the infinite sum (29b) by an equivalent difference equation

$$\sigma^x(t)=x(t)+R\sigma^x(t-T). \tag{30}$$

In the case of the EDFC, the averaged equation (8) for the complex amplitude takes the form

$$(2/\varepsilon)\dot{z}=-i\nu z-z(|z|^2-1)-\alpha-i\kappa[z-(1-R)\sigma_T^z], \tag{31a}$$

$$\sigma^z(t)=z(t)+R\sigma^z(t-T). \tag{31b}$$

Linearization of the system (31) around a periodic orbit yields the characteristic equation

$$\left(\frac{2\lambda}{\varepsilon}\right)^2-2(1-2s)\frac{2\lambda}{\varepsilon}+(3s-1)(s-1)+\left[\nu+\kappa\frac{1-e^{-\lambda T}}{1-e^{-\lambda T}R}\right]^2=0. \tag{32}$$

Formally this equation can be derived from Eq. (18) by the following replacement of the control term

$$(1-e^{-\lambda T})\Rightarrow(1-e^{-\lambda T})/(1-e^{-\lambda T}R). \tag{33}$$

Using an approximation $e^{-\lambda T}\approx 1-\lambda T$ the transcendental equation (32) can be transformed to the quadratic equation (19) with the renormalized value of the parameter K, which now is

$$K=\kappa T\varepsilon/2(1-R)=k\pi/\omega^2(1-R). \tag{34}$$

As a result the threshold of the Hopf bifurcation becomes

$$k_0=(1-R)\frac{\omega^2}{\pi\nu}\left(1-\frac{|A_0|^2}{2}\right). \tag{35}$$

Thus the increase of R causes the decrease of the lower threshold of stability proportionally to the multiplier $(1-R)$ [cf. Eqs. (35) and (23)].

The left-hand branch of FE is obtained from Eq. (25) by replacing k with $k(1-R)$

$$\mathrm{Re}\,\lambda=\frac{\varepsilon}{2}\frac{1-|A_0|^2/2-\nu k(1-R)\pi/\omega^2}{1+[k(1-R)\pi/\omega^2]^2}. \tag{36}$$

The equation for the right-hand branch of FE can be derived from Eq. (26) by using the replacement (33)

$$\lambda^2+\omega_0^2-k(1-e^{-\lambda T})/(1-e^{-\lambda T}R)=0. \tag{37}$$

Root loci diagram of this equation is shown in Fig. 7(b). Again the pair of complex conjugate roots intersects the imaginary axes at the points $\lambda=\pm i\pi/T=\pm i\omega/2$. The intersection appears for $k=k_1$, where

$$k_1=(1+R)\frac{1}{2}\left(\omega_0^2-\frac{\omega^2}{4}\right) \tag{38}$$

defines the upper threshold of stability for the EDFC. The increase of R causes the increase of the upper threshold proportionally to the multiplier $(1+R)$ [cf. Eqs. (38) and (27)].

Thus the EDFC extends the domain of stability by shifting both the lower threshold to the left and the upper threshold to the right. Domains of stability in the plane of parameters (k,R) are shown for two different periodic orbits in Fig. 8. We see that UPO with the parameters $(\nu,\alpha)=(0.25,0.3)$

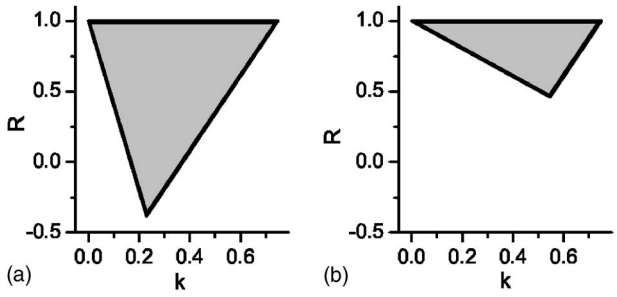

FIG. 8. Stability domains in the plane of parameters (k,R) for $\varepsilon=0.01$. The lower threshold is obtained from Eq. (35) and the upper threshold is determined from Eq. (38). (a) $(\nu,\alpha)=(0.9,0.6)$, (b) $(\nu,\alpha)=(0.25,0.3)$. The values of other parameters of the unstable orbits are presented in the captions of Figs. 6 and 9.

cannot be stabilized by the usual DFC. However its stabilization is possible by the EDFC with the parameter $R>0.46$.

To obtain an approximate analytical expression for the right-hand branch of FE we expand the solution of Eq. (37) in Taylor series close to the threshold $k=k_1$. As a result we get a modified Eq. (28)

$$\mathrm{Re}\,\lambda=\frac{(1-R^2)4\pi k_1/\omega}{(1+R)^4\omega^2+[(1-R)(2\pi k_1/\omega)]^2}(k-k_1), \quad (39)$$

where k_1 is defined by Eq. (38).

The validity of analytical results obtained in this section is demonstrated in Fig. 9. In Figs. 9(c) and 9(d) the leading FE's are presented for $R=0.5$ and the same values of parameters $(\nu,\alpha)=(0.9,0.6)$ as in Fig. 6. For small $\varepsilon=0.01$ [Fig. 9(a)], Eqs. (32) and (36) give quantitatively correct results for the left-hand branch, and Eq. (39) describes well the right-hand branch. Even for $\varepsilon=0.1$ [Fig. 9(b)], Eqs. (32) and (39) are in good agreement with the results obtained from exact variational equations, while Eq. (36) is less appropriate.

Comparing Figs. 9(a), 9(b), 6(a), and 6(c) we see that the EDFC indeed extends the domain of stability. Another property of the EDFC is that the optimal value of the control gain k_{op} is no longer determined by an intersection of the left-hand and right-hand branches of FE's, but by the minimum of the left-hand branch. Differentiating Eq. (36) with respect to k and equating the result to zero one can find an analytical expression for the optimal value of the control gain

$$k_{\mathrm{op}}=\frac{\omega^2(1-|A_0|^2/2)}{\nu(1-R)\pi}\left(1+\sqrt{1+\frac{\nu^2}{(1-|A_0|^2/2)^2}}\right). \quad (40)$$

As a last example in this section we consider a set of parameters $(\nu,\alpha)=(0.25,0.3)$ for which the system possesses three periodic orbits. We have shown that the smallest orbit cannot be stabilized by the usual DFC [see Fig. 8(b)]. We now consider a possibility of its stabilization by the EDFC. Figure 9(c) shows the left-hand branch of FE's obtained from transcendental Eq. (32) for different values of parameter R. An optimal value of this parameter that provides the deepest minimum in the dependence $\mathrm{Re}\,\lambda$ vs k is $R\approx 0.7$. In Fig. 9(c), the predicted values of the FE's are compared with the values of the Laypunov exponents determined from the exact

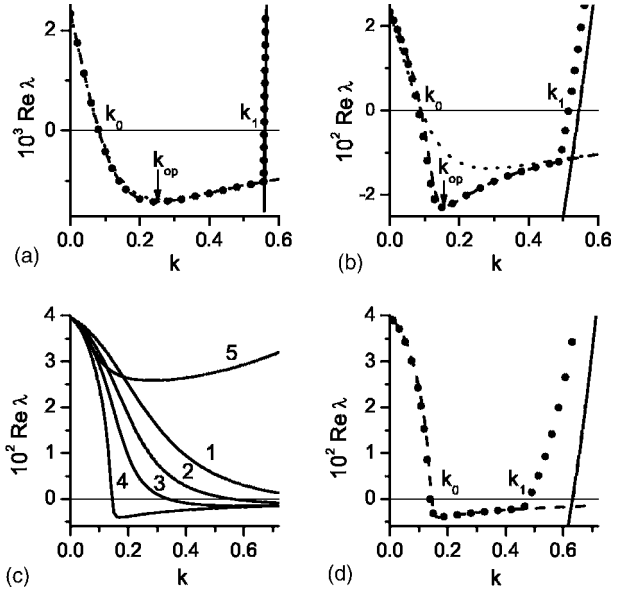

FIG. 9. Floquet exponents in the case of the EDFC. (a) and (b) Same diagrams as (a) and (c) in Fig. 6 but for $R=0.5$. (c) and (d) correspond to the set of parameters $\varepsilon=0.1$, $(\nu,\alpha)=(0.25,0.3)$, $\omega\approx 1.01258$, $a\approx 0.06075$, $|A_0|\approx 0.645$, and $\lambda_0\approx(3.96\pm 1.23i)\times 10^{-2}$. (c) Solution of transcendental Eq. (32) for different values of parameter R: (1) $R=0$; (2) $R=0.3$; (3) $R=0.5$; (4) $R=0.7$; (5) $R=0.9$. (d) Re λ vs k dependence for $R=0.7$. Solid dots are the values of the Lyapunov exponents obtained from exact variational equations (24) using replacement (29). The dashed and dotted lines determined, respectively, from Eq. (32) and Eq. (36) approximate the left-hand branch. The solid lines in (a), (b), and (d) obtained from Eq. (39) approximate the right-hand branches.

linearized equations for $R=0.7$. We see that this UPO can be stabilized with the UDFC provided the control gain is chosen from the interval $k_0<k<k_1$.

V. NUMERICAL DEMONSTRATIONS

To verify the validity of the linear theory we have numerically investigated the original nonlinear differential equations (2). For the set of parameter $(\nu,\alpha)=(0.6,0.9)$, $\varepsilon=0.1$ the results are presented in Fig. 10. Without control ($t<80T$) the van der Pol oscillator is not synchronized with the external force and a beat phenomenon is observed [Fig. 10(a)]. The DFC perturbation is switched on at the moment $t_c=80T$; it stabilizes an unstable UPO and we have a periodic motion synchronized with an external force [Fig. 10(b)]. Whenever the synchronization is established the feedback perturbation vanishes [Fig. 10(c)]. The envelopes of the transient are well described by the averaged amplitude equation (8). This confirms the validity of the averaging procedure applied to the time-delay system (2).

Figure 11 shows the dynamics of the system controlled by the extended delayed feedback for the set of parameter $(\nu,\alpha)=(0.25,0.3)$, $\varepsilon=0.1$, when the system possesses three periodic orbits. The largest orbit with the amplitude $|A_0|\approx 2.12$ is stable. It corresponds to the synchronized periodic motion of the system that is observed without control for t

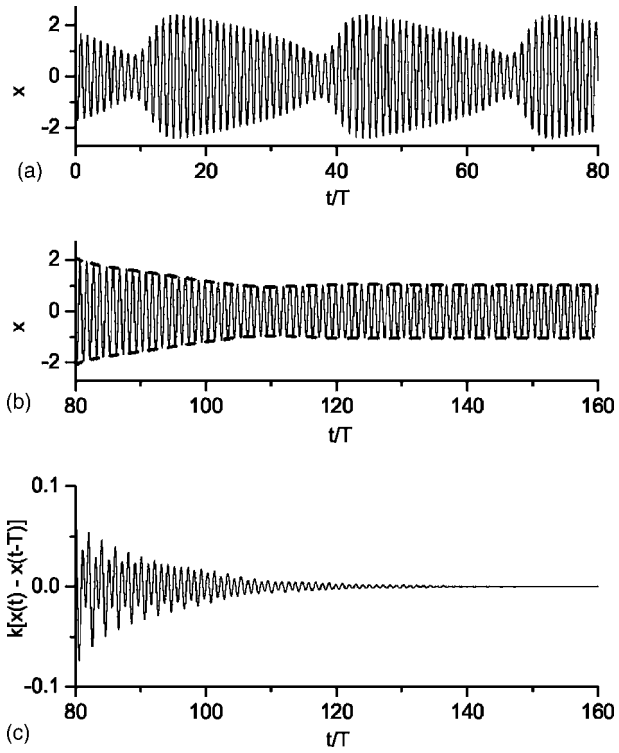

FIG. 10. Results of numerical integration of delay-differential equations (2) for $(\nu,\alpha)=(0.9,0.6)$, $\varepsilon=0.1$. (a) Dynamics of the x variable without control. (b) and (c) Dynamics of the x variable and perturbation $k[x(t)-x(t-T)]$ when the control is switched on. The broken line (an envelope) in (b) is the dynamics of the complex amplitude $|A(t)|=2|z(t)|$ obtained from averaged Eq. (8). The strength of the feedback gain is $k=0.34$; other parameters are the same as in Fig. 6(c).

$<t_c=50T$. The smallest orbit with the amplitude $|A_0| \approx 0.645$ is unstable; its two complex conjugate FE's are $\lambda_0 \approx (3.96\pm 1.23i)\times 10^{-2}$. The EDFC switches the system from synchronized motion with the large amplitude to another synchronized motion with the small amplitude. Whenever this new synchronization regime is established the feedback perturbation vanishes.

VI. CONCLUSIONS

We have developed an analytical approach for the delayed feedback control of a forced self-sustained oscillator close to a supercritical Hopf bifurcation. The analytical approach is based on an averaging method, a classical asymptotic method of nonlinear dynamics developed for weakly nonlinear oscillators. We have shown that this method works well even in the presence of the delayed feedback.

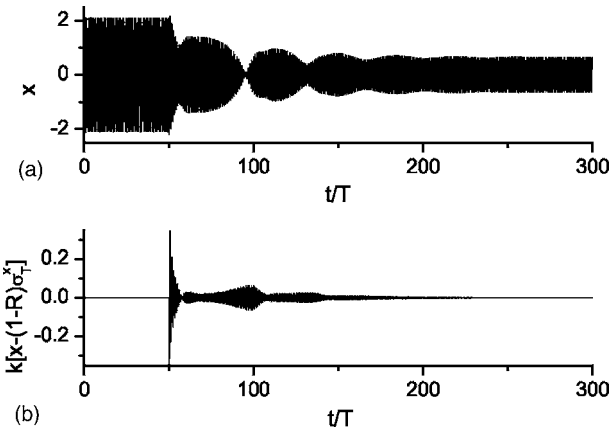

FIG. 11. Results of numerical integration of delay-differential equations (2) with the replacement (29) for $(\nu,\alpha)=(0.25,0.3)$, $\varepsilon=0.1$, $k=0.16$, and $R=0.7$. Other parameters are presented in the caption of Fig. 9. (a) Dynamics of the x variable. (b) Dynamics of the control perturbation $k[x-(1-R)\sigma_T^x]$. The control is switched on at the moment $t_c=50T$. The black regions are closely filled by oscillations.

Our analysis shows that the domain of synchronization of a forced self-sustained oscillator can be essentially extended by delayed feedback. This extension is based on the stabilization of the existing unstable periodic orbit and is attained with tiny control perturbations. The delayed feedback can be also used to change the synchronization regime from periodic oscillations with a large amplitude to periodic oscillations with a small amplitude.

In this paper, the delayed feedback control method is applied for the first time to control a quasiperiodic motion, i.e., the motion on a torus in the phase space. The unstable periodic orbits in this case have a pair of complex conjugate Floquet multipliers outside the unit circle in the complex plane.

The analytical approach is demonstrated for the paradigmatic model of the forced van der Pol oscillator. We have obtained simple analytical expressions for the dependence of leading Floquet exponents on the control gain and determined the lower and upper threshold of stability as well as an optimal value of the control gain. We have also determined analytical properties of the extended delayed feedback controller. The main results and the approach are of general importance since they are relevant to any forced self sustained oscillator close to the supercritical Hopf bifurcation. We believe that the developed analytical approach is an important contribution to the theory of the delayed feedback control.

[1] K. Pyragas, Phys. Lett. A **170**, 421 (1992).
[2] *Handbook of Chaos Control*, edited by H. G. Shuster (Wiley-VCH, Weinheim, 1999).
[3] K. Pyragas, in *Synchronization: Theory and Application*, edited by A. Pikovsky and Yu. Maistrenko (Kluwer, Dordrecht, 2003), pp. 187–219.
[4] K. Pyragas and A. Tamaševičius, Phys. Lett. A **180**, 99 (1993); A. Kittel, J. Parisi, K. Pyragas, and R. Richter, Z. Naturforsch., A: Phys. Sci. **49a**, 843 (1994); D. J. Gauthier, D. W. Sukow, H. M. Concannon, and J. E. S. Socolar, Phys. Rev. E **50**, 2343 (1994); P. Celka, Int. J. Bifurcation Chaos Appl. Sci. Eng. **4**, 1703 (1994).
[5] T. Hikihara and T. Kawagoshi, Phys. Lett. A **211**, 29 (1996); D. J. Christini, V. In, M. L. Spano, W. L. Ditto, and J. J. Collins, Phys. Rev. E **56**, R3749 (1997).
[6] S. Bielawski, D. Derozier, and P. Glorieux, Phys. Rev. E **49**, R971 (1994); M. Basso, R. Genesio R, and A. Tesi, Syst. Control Lett. **31**, 287 (1997); W. Lu, D. Yu, and R. G. Harrison, Int. J. Bifurcation Chaos Appl. Sci. Eng. **8**, 1769 (1998).
[7] T. Pierre, G. Bonhomme, and A. Atipo, Phys. Rev. Lett. **76**, 2290 (1996); E. Gravier, X. Caron, G. Bonhomme, T. Pierre, and J. L. Briancon, Eur. Phys. J. D **8**, 451 (2000); Th. Mausbach, Th. Klinger, A. Piel, A. Atipo, Th. Pierre, and G. Bonhomme, Phys. Lett. A **228**, 373 (1997).
[8] T. Fukuyama, H. Shirahama, and Y. Kawai, Phys. Plasmas **9**, 4525 (2002).
[9] O. Lüthje, S. Wolff, and G. Pfister, Phys. Rev. Lett. **86**, 1745 (2001).
[10] P. Parmananda, R. Madrigal, M. Rivera, L. Nyikos, I. Z. Kiss, and V. Gaspar, Phys. Rev. E **59**, 5266 (1999); A. Guderian, A. F. Munster, M. Kraus, and F. W. Schneider, J. Phys. Chem. A **102**, 5059 (1998).
[11] H. Benner and W. Just, J. Korean Phys. Soc. **40**, 1046 (2002).
[12] J. M. Krodkiewski and J. S. Faragher, J. Sound Vib. **234**, 591 (2000).
[13] K. Hall, D. J. Christini, M. Tremblay, J. J. Collins, L. Glass, and J. Billette, Phys. Rev. Lett. **78**, 4518 (1997).
[14] J. E. S. Socolar, D. W. Sukow, and D. J. Gauthier, Phys. Rev. E **50**, 3245 (1994).
[15] K. Pyragas, Phys. Lett. A **206**, 323 (1995).
[16] K. Pyragas, Phys. Rev. Lett. **86**, 2265 (2001).
[17] K. Pyragas, V. Pyragas, and H. Benner, Phys. Rev. E **70**, 056222 (2004).
[18] H. Nakajima, Phys. Lett. A **232**, 207 (1997).
[19] W. Just, T. Bernard, M. Ostheimer, E. Reibold, and H. Benner, Phys. Rev. Lett. **78**, 203 (1997).
[20] K. Pyragas, Phys. Rev. E **66**, 026207 (2002).